Low-frequency noise in serial arrays of MgO-based magnetic tunnel junctions

Wenzhe Zhang,* Qiang Hao, and Gang Xiao†
Department of Physics, Brown University, Providence, Rhode Island 02912, USA
(Received 27 March 2011; revised manuscript received 3 June 2011; published 27 September 2011)

We have studied the low-frequency noise in MgO-based magnetic tunnel junctions (MTJs) in serial configurations. Two types of junctions were compared: MTJ Wheatstone bridges and MTJ discrete resistors closely packed on a wafer die. We have characterized each individual junction to ensure that they have uniform parameters such as linear field sensitivity and noise level. In the array of bridges, the low-frequency noise decreases with an increasing number (N) of bridges, but does not scale with $1/\sqrt{N}$, as expected from noise theory. The deviation is likely due to the statistical dispersions in MTJ bridge resistance and normalized voltage noise. The total noise of the discrete resistor series does not scale with $1/\sqrt{N}$ either, but rather exhibits a sinusoidal-like variation with N. We attribute it to the possible enhancement of noise from magnetic coupling among the tightly spaced MTJ elements.

DOI: 10.1103/PhysRevB.84.094446 PACS number(s): 73.50.Td, 85.30.Mn, 75.76.+j, 85.75.−d

I. INTRODUCTION

Magnetic tunnel junctions (MTJs) have increasingly been used as magnetic field sensing devices due to their very large tunneling magnetoresistance (TMR) at room temperature.[1,2] In general, sensitive MTJ sensors require not only large output voltages but also large signal-to-noise ratios (SNRs). Therefore, diminishing the noise becomes as important as raising the TMR signal outputs. For MTJ devices that operate at high frequency, white noise with a frequency-independent power distribution determines the minimum noise level. White noise includes thermal (Johnson) noise and shot noise, which are due to two distinct mechanisms. At low frequency, the $1/f$ noise and sometimes random telegraph noise (RTN) dominate in the noise spectrum. RTN is characterized by output voltage fluctuations between two levels,[3] exhibiting a Lorentzian-type frequency spectrum. Since RTN is strongly dependent on particular bias voltages and can be minimized by proper annealing procedures, the main low-frequency noise is of the $1/f$ type, namely, with the spectral power density inversely proportional to the frequency.

In MgO-based MTJs, the $1/f$ noise arises from the interaction of tunneling electrons with defects in the barrier (nonmagnetic origin)[4] and the fluctuations in the ferromagnetic structures, e.g., the free-layer (magnetic origin).[5] Several techniques have been used to enhance the field detection, for instance, using a microelectromechanical component (a flux concentrator) that shifts the MTJ operating frequency to higher frequencies where the $1/f$ noise can be one or two orders of magnitude smaller[6,7] or using discrete tunnel junctions connected in series or parallel.[8,9] The objective of this paper is to reduce the $1/f$ noise in two distinct types of MTJs by arranging each type in their own serial arrays.

II. EXPERIMENT

We deposited MTJ multilayer films on thermally oxidized silicon wafers using a custom multitarget high-vacuum magnetron sputtering system (base pressure of 2×10^{-8} Torr). The MTJ stack has the following structure (thicknesses in angstroms): 50 Ta/300 Ru/50 Ta/20 CoFe/150 IrMn/20 CoFe/8 Ru/30 CoFeB/20.5 MgO/FL/50 Ta/100 Ru. The free-layer (FL) consists of 30 CoFeB/600 Conectic for one type of sample called the bridge sensor, and 600 CoFeB for another called the resistor sensor. All layers except the MgO barrier were deposited by dc sputtering at a constant Ar pressure of 2.05 mTorr. The MgO barrier was deposited through rf magnetron sputtering at an Ar pressure of 1.1 mTorr. During the sputtering process, the substrates were rotated at a constant speed to maximize uniformity throughout each wafer. Junctions were patterned using the standard photolithography and ion-beam milling process (the detailed pattern and geometry of the bridge sensor and resistor sensor will be given later). After deposition and patterning, the MTJs were annealed at 310 °C for 4 h at 8×10^{-8} Torr in an applied magnetic field of 4.5 kOe, in order to define the intrinsic magnetic axis and to achieve a high magnetoresistance ratio through crystallization of the amorphous CoFeB layers.

We performed magnetic sensitivity measurements in orthogonal magnetic fields applied along the sensing (H_E) and biasing direction (H_B) of the MTJ sensors. The transfer curves (resistance versus field) were obtained by recording the resistance values from the MTJs under a sweeping of H_E in a descending and ascending manner. Additionally, we measured the field sensitivity by adding a modulating ac field on H_E. We generated a small ac field ($\delta H \sim 1$ Oe) along the sensing direction of the MTJs by using a Helmholtz coil. The ac voltage output from the MTJ (δV), in response to δH, was measured by using a lock-in amplifier as H_E was swept.[10] The noise measurements were carried out in an electromagnetically shielded box. We used batteries to power the MTJs to minimize noise in the setup. We used a two-channel time cross-correlation method to measure the noise spectrum from the MTJs. The signal from each signal was boosted by an amplifier with an intrinsic noise of 1.3 $\mathrm{nV/Hz^{1/2}}$ at 1 Hz, and fed into a two-channel dynamic spectral analyzer (HP 35670A).

The noise spectrum we acquired can be described by the following equation:

$$S_v = 2\mathrm{eV}R\coth\left(\frac{\mathrm{eV}}{2k_BT}\right) + \frac{\alpha V^2}{Af^\gamma}, \tag{1}$$

where the first term represents the thermal and shot noise and the second one the $1/f$ noise. In Eq. (1), V is the bias voltage,

R the resistance, e the electron charge, k_B the Boltzmann constant, and T the temperature. When $eV \ll k_BT$, the usual thermal (Johnson) noise relation is obtained. The shot-noise relation is obtained when the $\coth(eV/2k_BT)$ term approaches unity at higher voltages ($V \sim 150$ mV). In the second term, A is the area of the junction, f the frequency, γ the exponent (usually around 1), and α the Hooge-like parameter.[11]

III. RESULTS AND DISCUSSIONS

A. The case of MTJ bridges

The first type of MTJ device that we studied is a Wheatstone bridge magnetic sensor as shown in the inset (I) of Fig. 1(a). Each monolithic sensor fabricated using a standard photolithography process consists of four arms on a silicon wafer of $\sim$1 mm^2. The two sensing arms in the bridge respond to the external field linearly, whereas the two reference arms remain inert to the field. Both the sensing arms and reference arms are composed of multiple MTJ elements (22 in each arm with lateral dimension 50×20 μm), with adjacent MTJ elements connected to each other alternately through the bottom or top electrical leads. The elements in the two black squares are included in the reference arms, and all MTJ elements are spaced 90 μm apart. The magnetic easy axes of the sensing units are set (by shape anisotropy) to be perpendicular to those of bottom pinned layer. In the serial connection setting, only V_B terminals are used, as shown in the inset (II) of Fig. 1(a).

Figure 1(a) shows the linear transfer curve (bridge resistance versus external magnetic field) for a representative MTJ bridge sensor. When the MTJ bridge is saturated, both of the reference arms and sensing arms will be aligned along the external field. The reference arm will yield a square-shaped hysteresis loop on top of the linear field response of the sensing arm. For most sensing applications, a MTJ bridge operates within its linear range (-10 to 10 Oe), and the magnetization of the reference arms remains unaltered. A typical value for the saturated TMR is 45%. Figure 1(b) gives the spectral power density of a representative MTJ measured at 1 V. Figure 1(c) shows the $1/f$ voltage noise measured at 1 Hz as a function of the bias voltage to the bridge sensor. The voltage noise is the square root of noise spectral density S_v. As expected from Eq. (1), this $1/f$ voltage noise scales linearly with V, with a small residual noise (the intercept) of 0.211 μV/Hz$^{1/2}$ at $V = 0$. We can normalize the voltage noise by V to get the normalized voltage noise $\sqrt{S_v}/V$ or S_n, which is the voltage noise at 1 V.

Since only V_B terminals are used for the noise measurements, each MTJ bridge is composed of two legs connected in parallel and each leg comprises 44 junctions in a series. The total bias voltage ranges from 0.3 V to 1.2 V across a bridge, equivalent to 6.8 mV to 27.2 mV across a single junction, which is approximately the same magnitude as k_BT. In this energy range, bias-independent tunneling process dominates, leading to a low variance of the Hooge-like parameter.[12–14] As shown in Fig. 1(d), the power density at 1 Hz versus bias for a single junction is a slightly downward sloping curve, in consistency with the reports on the Hooge-like parameter published earlier.[12] The variance of the Hooge-like parameter can be characterized by the variability of the least-squares estimates of the regression parameters. As shown in Fig. 1(e), we present the averaged voltage noise at 1 Hz of a single junction as a function of the voltage. The standard error for a least-squares (LS) estimate of the slope is 7.6×10^{-7} Hz$^{-0.5}$,

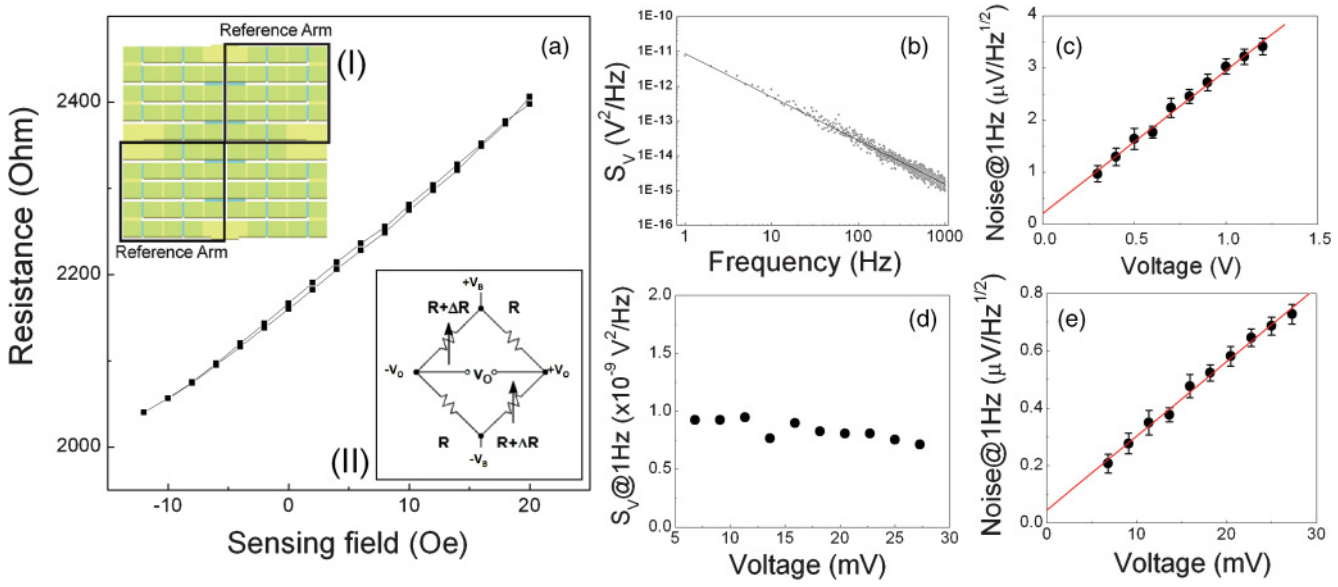

FIG. 1. (Color online) (a) Resistance of a representative MTJ bridge sensor versus external (sensing) field. This transfer curve is nearly linear and has a small hysteresis. The resistance is measured between the V_B terminals of the bridge. Inset (I) shows the schematics of a MTJ bridge with adjacent MTJ elements connected to each other through the bottom and top leads, and the sections in black squares are included in the reference arms. Inset (II) shows the equivalent circuit diagram of the bridge. (b) Noise spectrum (spectral power density S_v) for a representative MTJ measured at 1 V. (c) The voltage noise (at 1 Hz) of the bridge as a function of bias voltage. A linear fit shows a slope of 2.745×10^{-6}/Hz$^{1/2}$ and a small intercept of 0.211 μV/Hz$^{1/2}$ at $V = 0$. (d) The power density at 1 Hz versus applied bias for a single element. (e) The averaged voltage noise (at 1 Hz) of a single element as a function of bias voltage.

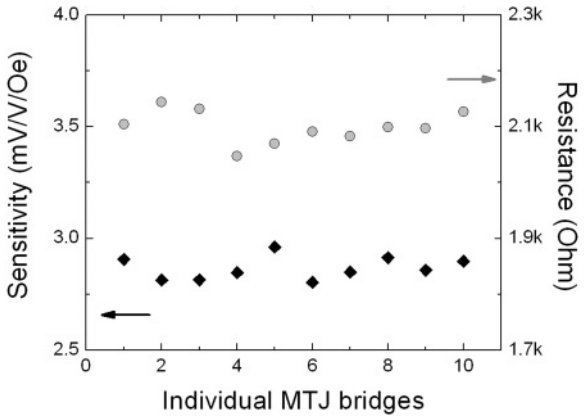

FIG. 2. We used ten MTJ bridge sensors in our study. The sensitivity and zero-field resistance of all the sensors are similar as shown here. The average sensitivity is 2.87 mV/V/Oe, with a standard deviation (σ) of 0.06. The average resistance is 2100 Ω with σ of 29.6.

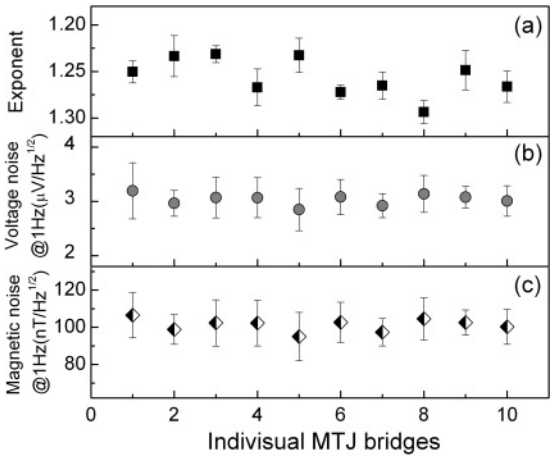

FIG. 3. (a) The exponent (γ) of $1/f$ noise of the ten MTJ bridge sensors used in this paper. The error bar represents the experimental error from the ten spectra taken for each sensor. The distribution of the exponent for these ten junctions has a mean (μ) of 1.25 and a standard deviation (σ) of 0.02. (b) Normalized voltage noise at 1 Hz. The distribution has μ of 3.0 and σ of 0.2. (c) Magnetic field noise at 1 Hz. The distribution has μ of 101.2 and σ of 3.2.

or 3% of the fitted slope (2.6×10^{-5}) $\mathrm{Hz}^{-0.5}$, meaning a low variance of the Hooge-like parameter. Similarly, the parameter estimate for the intercept is 44.6 $\mathrm{nV/Hz^{0.5}}$, with a standard error for LS estimate being 13.9 $\mathrm{nV/Hz^{0.5}}$. One can use the t-test to claim that the intercept is significantly different from 0 at the 95% confidence level (t-statistic = 3.2). The above analysis has shown that the residual noise is intrinsic to the MTJ bridge, and cannot be explained away by the small variance of the Hooge-like parameter.

We have also measured the field sensitivity of individual bridge sensors. The sensitivity parameter s is defined as the ratio of the output sensing voltage to the input voltage under a 1 Oe field change, i.e., $s = (\delta V/\delta H)/V$. Equivalently, s is the same as the relative change in bridge resistance (R) or in conductance (G) of 1 Oe magnetic field. According to the magnetotunneling theory $G = G_0[1 + P^2 \cos\theta_F]$, where G_0 is a constant, P is the spin polarization and θ_F is the orientation of the magnetization of the free-layer relative to that of the pinned layer. In term of G, the s parameter can be expressed as

$$s \equiv \frac{1}{G}\frac{\delta G}{\delta H} = \frac{1}{G_0[1 + P^2\cos\theta_F]}\frac{G_0 P^2 \delta(\cos\theta_F)}{\delta H} = \frac{P^2}{[1 + P^2\cos\theta_F]}\frac{\delta(\cos\theta_F)}{\delta H}. \quad (2)$$

The sensitivity and the resistance of the ten bridge sensors used in this paper have low variances as shown in Fig. 2.

We have characterized noise behaviors of all the bridge sensors by measuring their noise spectra. Using Eq. (1), we are able to extract the exponent and voltage noise values from MTJ noise spectra. Additionally, we have derived the field detectability of each bridge sensor. The detectability is characterized by the intrinsic field noise value S_H, which is equal to S_n/s, where S_n is the normalized voltage noise and s is the sensitivity parameter. Figure 3 shows the $1/f$ noise exponent, the voltage noise (at 1 Hz), and the magnetic field noise S_H (at 1 Hz). Again, the low variances in all the noise data suggest that all the MTJ bridge sensors have rather uniform noise properties and performance.

Next, we connect these bridge sensors in series with the notation N-bridge, which represents the N-bridge sensors in a series. All MTJ bridges are spaced 10 mm apart. Figure 4 shows the evolution of the exponent, voltage noise (at 1 Hz), and magnetic noise (at 1 Hz) as functions of the number (N) of bridge sensors in a series. In the present research, we only employed ten MTJ bridges. In fact, each bridge consists of two legs connected in parallel and each leg comprises 44 junctions in series, i.e., it is a 44×2 junction network. An array of ten MTJ bridges is equivalent to a network of 440×2 junctions. It can be seen in Fig. 4 that the series connection does not affect the noise exponent, but consistently reduces the noise level as N increases.

The reduction in noise with an increasing N is inconsistent with the behavior of $1/f$ noise [see the red dashed lines in Figs. 4(b) and 4(c)]. In our case, each of the bridge sensors in a series can be considered as an independent noise source. The noise power from each bridge sensor is $\frac{\alpha V_{\mathrm{tot}}^2}{N^2 A f^\gamma}$ (V_{tot} is the total voltage across the whole series, fixed at 1 V), the total voltage noise of the series is therefore $\sqrt{N[\frac{\alpha V_{\mathrm{tot}}^2}{N^2 A f^\gamma}]}$, which should scale as $1/\sqrt{N}$. MTJ bridges included in each array all have similar resistance (R—see Fig. 2) and similar normalized voltage noise [S_n—see Fig. 3(b)]. However, the small dispersions in R and S_n may still result in the slight deviation of the total noise from the assumed $1/\sqrt{N}$ model.

Let us first consider the dispersion of R only. If one fixes the total voltage bias to 1 V and chooses a constant voltage noise S_n, the noise power of an N-bridge array can be described as $\sum_{i=1}^{N}(S_n V_i)^2$, where V_i is the voltage drop on each bridge with the constraint $\sum_{i=1}^{N} V_i = 1$. The dispersion in R will translate into the dispersion of V_i. By invoking the inequality relation $V_1^2 + V_2^2 + \cdots + V_N^2 \geqslant N[(V_1 + V_2 + \cdots + V_N)/N]^2$, we know that the total voltage noise is sure to be larger than $S_n/\sqrt{N}$. Next let us consider the dispersion of S_n, i.e., each MTJ bridge has its own

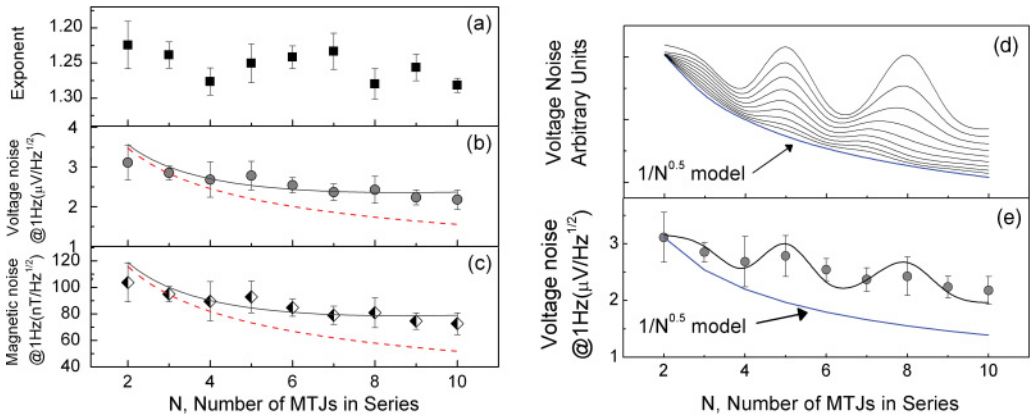

FIG. 4. (Color online) (a) The exponent (γ) of noise of an N-bridge as a function of the number (N) of bridge sensors in series. (b) Normalized voltage noise at 1 Hz. (c) Magnetic field noise at 1 Hz. The predictive lines in (b) and (c) are obtained using the formula of the form $[pN + q/N]^{1/2}$ (black solid line) and $\sqrt{1/N}$ (red dashed line), where p and q are the fitting parameters. (d) shows the incremental increase in the deviation from the baseline model based on different magnitudes of dispersions in R and S_n. (e) We fit the normalized voltage noise (b) with one model selected from (d).

normalized voltage noise S_{ni} but has the same resistance. The noise power becomes $\sum_{i=1}^{N}(S_{ni}/N)^2$. Again, by invoking the inequality relation $S_{n1}^2 + S_{n2}^2 + \cdots + S_{nN}^2 \geqslant N[(S_{n1} + S_{n2} + \cdots + S_{nN})/N]^2$, we know that the total voltage noise is sure to be large than $\overline{S_n}/\sqrt{N}$.

Based on our simulations, we have plotted the incremental increase in the deviation of total noise from the $1/\sqrt{N}$ model over different magnitude of dispersions in R and S_n, as shown in Fig. 4(d). The baseline model is marked by the arrow. We selected the best model to fit the normalized voltage noise as seen in Fig. 4(e). Within the experimental error, the measured voltage noise is in a fair agreement with the expectation (black solid line). During the computer simulations, we have set the seed of the pseudorandom number generator (thus fixing the shape of the fitting curve) to make the results repeatable and to achieve the best fitting.

To simplify the fitting formula, we added a constant noise term S_c (due to the dispersion) to the basic $1/\sqrt{N}$ model, then the noise power of the serial MTJ array (N bridge) can be described as $N[\frac{\alpha V_{\text{tot}}^2}{N^2 A f^\gamma}] + NS_c$. If we fix the total voltage bias to 1 V, then the simplified equation for the noise spectral density is $pN + q/N$, where p and q are the parameters to be determined by a standard regression analysis. The R-square value, which defines the proportion of the total variance explained by the model (also used as an indicator of how well the model fits the data), is 98.25%. We presented the fitted data in Figs. 4(b) and 4(c) (see the black solid lines). It has shown that the formula successfully captures the tendency of total noise to decrease over increasing N as well as the deviation from the standard model because of the dispersions in R and S_n.

B. The case of MTJ discrete resistors

In comparison, we have also studied another type of MTJ sensors: serially connected MTJ discrete resistors. Within a 1 mm^2 area of silicon wafer, we patterned 20 MTJ elements connected in series, as shown in Fig. 5(a). The elements are spaced 100 μm apart, and have an oval shape (50 μm × 90 μm), with the longer axis as the magnetic easy axis. The sensing field is applied along the shorter axis. Figure 5 shows the TMR curve for a sensor consisted of 20 MTJ discrete resistors connected in a series. The saturated tunneling magnetoresistance (TMR) is 58%. The resistance is linear in field with a small hysteresis. Figure 5(b) shows the voltage noise at 1 Hz of a discrete resistor as a function of the bias voltage. The voltage noise of the MTJ resistor ($S_v^{0.5}$) is a linear function of applied bias. The Hooge-like parameter is practically constant in the explored range of voltages (V = 0.1–1V). To ensure that these MTJ sensors are uniform on parameters such as field sensitivity and resistance, we carried out similar measurements as described previously. In Fig. 6, the left-hand axis shows the sensitivity of individual MTJ junctions used in this paper. The right-hand axis gives their resistance in the absence of magnetic fields. Only a portion of the 20 MTJs was selected for this type of measurement.

Under an external sensing field, the magnetization vector in the free-layer rotates away from the easy (longer) axis. Simultaneously, we measured the low-frequency noise at 1 Hz

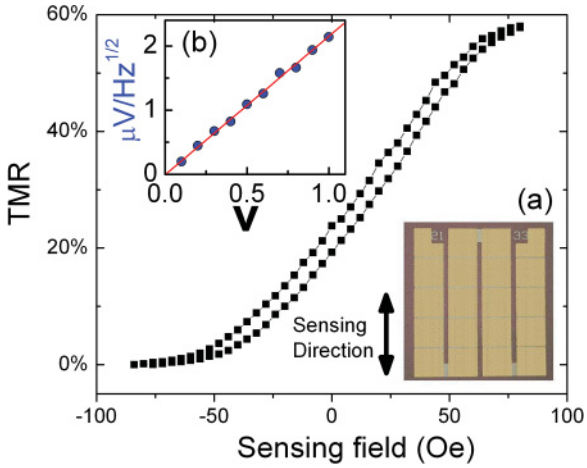

FIG. 5. (Color online) TMR curve of a MTJ sensor consisting of 20 MTJ discrete resistors. This sample is used for our noise study. (a) is a photograph of the MTJ sensor die measuring ~1 mm^2 in area. (b) shows the voltage noise at 1 Hz of a discrete resistor as a function of the voltage bias.

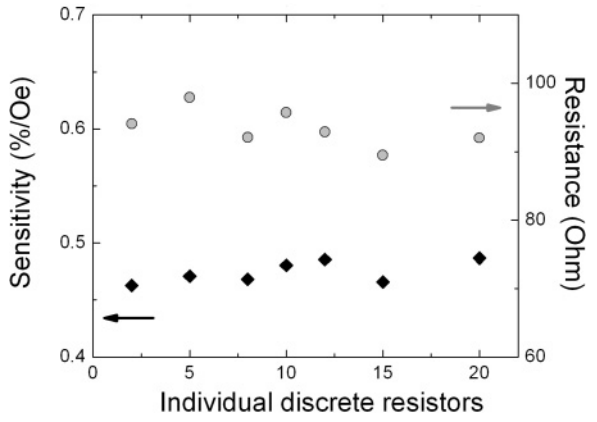

FIG. 6. Sensitivity parameter and resistance of individual MTJ discrete resistors. The average sensitivity is 0.47%/Oe (σ of 0.01%/Oe). The average resistance is 93.4 Ω (σ of 2.7).

and the sensitivity as a function of sensing field (−80 to 80 Oe). Figure 7(a) shows the results of a representative sensor. As can be seen, the voltage noise and sensitivity parameters are strongly correlated, as well as being field dependent. Therefore, the low-frequency noise clearly originates from magnetic fluctuations in the free layer. Figure 7(b) shows

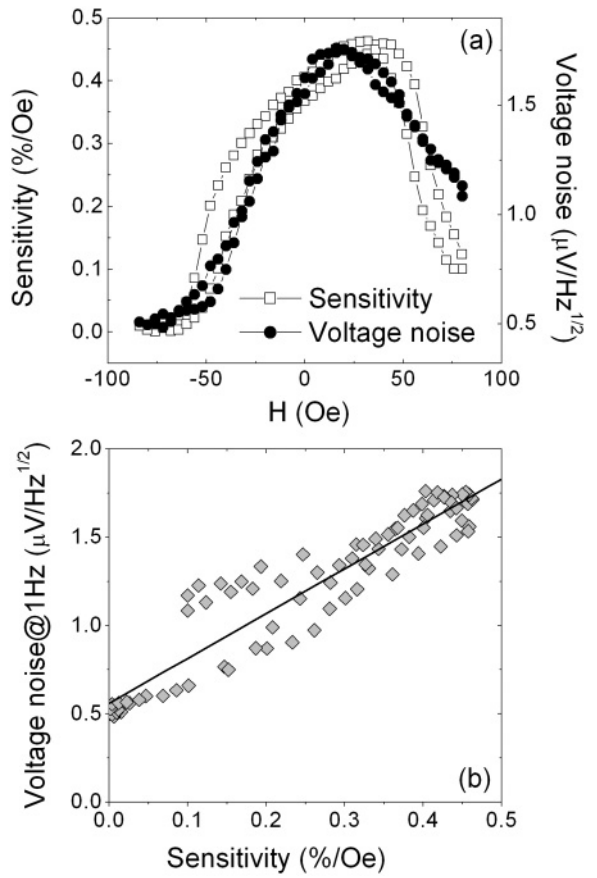

FIG. 7. (a) Magnetic field dependence of the sensitivity parameter and the voltage noise for a MTJ sensor with 20 MTJ discrete resistors in series. (b) Correlation between voltage noise at 1 Hz and sensitivity parameter. A linear fit yields a slope of 25.4 nT/Hz$^{1/2}$ and an intercept of 560 nV/Hz$^{1/2}$.

the linear correlation between the normalized voltage noise measured at 1 Hz and the sensitivity (s). A linear fit to the data yields a slope of 25.4 nT/Hz$^{1/2}$ at 1 Hz, and an intercept of 560 nV/Hz$^{1/2}$ as s approaches zero. Our interpretation is that the intercept is the residual noise from nonmagnetic contributions, such as defects or carrier traps in the barrier. On the other hand, the slope is due to the intrinsic magnetic noise. The larger is the field sensitivity, the larger is the noise. A MTJ is just a voltage output device dictated largely by the spin states of the free layer. The ratio of the magnetic to nonmagnetic noise is ∼3, indicating the dominance of the magnetic noise in our MTJs.

In many MTJ and GMR (giant magnetoresistance) devices, magnetization noise has been seen to scale linearly with the field sensitivity.[15–17] Physically speaking, sensitivity is a coupling parameter between the magnetic fluctuations in the free layer to the output voltage noise. To see this mathematically, the magnetic noise (S_H) can be expressed as

$$S_H = \delta V/(Vs) = (1/s)(1/V)(\delta V/\delta H)(\delta H/\delta m)\delta m_s = \delta m_s/\chi, \quad (3)$$

where δm_s represents the magnetization fluctuation noise, χ is the magnetic susceptibility, $\delta m_s/\delta H$, and $s = 1/V(\delta V/\delta H)$. We can estimate χ using Eq. (2). In our case $\theta_F \approx \frac{\pi}{2}$ (orthogonal magnetic orientation between the free layer and the pinned layer in the sensing mode), Eq. (2) becomes

$$s \approx \frac{P^2}{m_s}\frac{\delta(m_s\cos\theta_F)}{\delta H} = \frac{P^2}{m_s}\chi. \quad (4)$$

The spin polarization P is estimated using Julliere's model according to TMR $\equiv \frac{G_P - G_{AP}}{G_{AP}} = \frac{2P^2}{1-P^2}$, or $P = \sqrt{\frac{\text{TMR}}{2+\text{TMR}}} = 0.47$. Putting everything together, and using $s = 0.41\%/\text{Oe}$ ($H_E = 0$ Oe),

$$S_H = \frac{\delta m_s}{m_s}\frac{P^2}{s} \approx \frac{\delta m_s}{m_s}5.5\ \text{mT}, \quad (5)$$

where $\frac{\delta m_s}{m_s}$ is the transverse magnetization of the free layer normalized to its saturation magnetization.[18,19] For a MTJ with magnetic field noise up to 60 nT/Hz$^{1/2}$ at 1 Hz, this converts into $\frac{\delta m_s}{m_s} \sim 0.001\%$.

In Fig. 8 we show the evolution of (a) the $1/f$ exponent, (b) the voltage noise at 1 Hz, and (c) the magnetic field noise at 1 Hz as functions of the number (N) of discrete junction resistors in a series (all at zero field). The noise measurement for N-series MTJs is performed at zero fields because the field sensitivity of the MTJ device is close to its maximum in that range. The magnetic field noise (detectability) is defined as the ratio of voltage noise to field sensitivity. The best detectability is achieved when the external magnetic field is close to zero bias field. In addition, for most of the MTJ sensing applications, devices are integrated into the measurement system without an adding extra dc bias field, and the voltage noise at zero bias field is used as a specification when gauging magnetic sensing capabilities.

While the $1/f$ exponent is similar to that obtained in the case of bridge sensors, the N-dependence of low-frequency noise is different. As shown in Figs. 8(b) and 8(c), a spline line connecting the magnetic noise data shows a sinusoidal-like

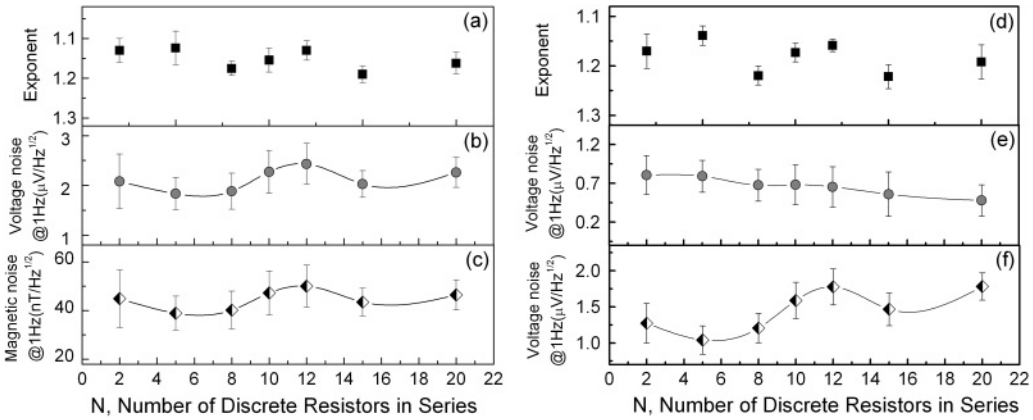

FIG. 8. (a) The exponent of $1/f$ noise, (b) the normalized voltage noise at 1 Hz, and (c) the low-frequency magnetic noise at 1 Hz, for a MTJ sensor consisting of N discrete resistors. The applied bias voltage is 1 V across the MTJ sensor. (d)–(f) show the noise behavior for a MTJ resistor in a saturation field. (d) shows the exponent of $1/f$ noise, (e) the normalized voltage noise in a saturation field of 80 Oe, and (f) the numeric difference between (b) (at zero fields) and (e) (at 80 Oe) in the unit of $\mu V/Hz^{0.5}$.

variation of magnetic noise with N, rather than a decrease of $1/\sqrt{N}$, as would be expected from noise theory. The constant noise term S_c as discussed in the last section will only increase with N, therefore it cannot be responsible for the noise bulge in Fig. 8(c). The scaling of $1/\sqrt{N}$ assumes that all the MTJ elements in a series are magnetically independent. Such an assumption may not hold in our case. We conjecture that the sinusoidal-like variation may originate from the magnetic coupling among the tightly spaced MTJ elements on a tiny silicon die ($\sim$1 mm^2).

To confirm that the noise enhancement indeed arises from the magnetic coupling, we performed additional noise measurements on discrete resistors in a saturation field. This allows us to separate magnetic and nonmagnetic noise, and test the $1/\sqrt{N}$ dependence of noise in the absence of magnetic noise. We presented the results in Figs. 8(d)–8(f), where Fig. 8(d) shows the exponent of $1/f$ noise, Fig. 8(e) the normalized voltage noise in a saturation field of 80 Oe, and Fig. 8(f) the numeric difference between Figs. 8(b) (at zero fields) and 8(e) (at 80 Oe) in units of $\mu V/Hz^{1/2}$. The nonmagnetic noise, which can be interpreted as the intercept in Fig. 7(b), is dominant in Fig. 8(e). The magnetic noise, including the magnetic fluctuation in the free layer and magnetic coupling, exhibits a sinusoidal-like variation, as shown in Fig. 8(f).

To estimate the magnitude of the magnetic coupling, we consider 5×4 ($\mathbf{y}$ and $\mathbf{x}$ axes) arrays of elliptical free-layer elements to mimic our real sensor die, each with magnetic moment $\mathbf{m_s}$. The elements are arranged on a rectangular lattice with a lattice spacing of a along the $\mathbf{x}$ axis and b along the $\mathbf{y}$ axis, specified with a position vector $\mathbf{r_{ij}} = ai\mathbf{e}_x + bj\mathbf{e}_y$, where i and j are integers, and $\mathbf{e}_x$ and $\mathbf{e}_y$ are unit vectors along the axes. In our sample, a and $b \sim 100$ μm [see Fig. 5(a)]. The magnetic coupling field on an element at $\mathbf{r_{ij}}$ is given by

$$\mathbf{H_{ij}} = \sum_{p,q\neq i,j} \frac{\mu_0}{4\pi} \frac{[3(\mathbf{m_s}\cdot\mathbf{n})\mathbf{n} - \mathbf{m_s}]}{r^3}, \qquad (6)$$

where $\mathbf{n}$ and r are the unit vector and norm for $(\mathbf{r_{ij}} - \mathbf{r_{pq}})$, respectively. In our case, the magnetic moments are aligned along the easy axis (i.e., $\mathbf{x}$ axis). We have calculated the coupling fields in Eq. (6) and displayed the vectors (with amplitude and direction) in the inset (right-hand side) of Fig. 9.

Because of the coupling field, the magnetic fluctuations of all the neighboring elements will be experienced by the element at $\mathbf{r_{ij}}$, creating an additional voltage noise on this element. According to our calculation (with CoFeB saturated magnetization being 1100 emu/cm^3), the average coupling field is of the order of 0.8 Oe. Earlier, we estimated that the magnetic fluctuation of each element along the sensing axis is $\frac{\delta m_s}{m_s} \sim 0.001\%$. Therefore the coupling field fluctuation, due to the magnetic fluctuation of all neighboring elements, can generate an extra field noise up to the order of 0.2 $\mu V/Hz^{1/2}$, or 10% of the normalized voltage noise 2 $\mu V/Hz^{1/2}$ as seen in Fig. 8(b). Because the coupling field for each element

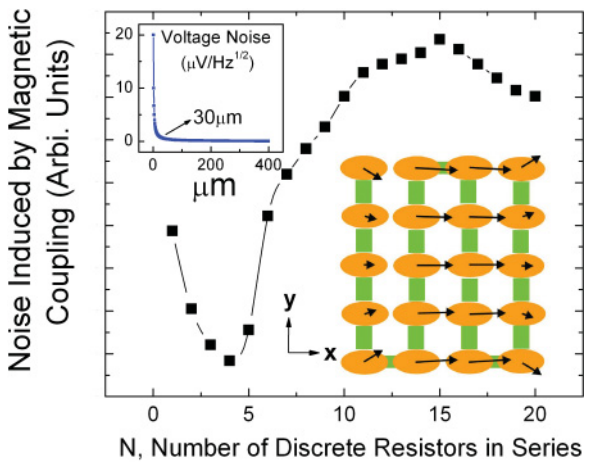

FIG. 9. (Color online) The estimated magnetic noise of a series of N-MTJ resistors, due to magnetic couplings among all MTJ elements. The total applied voltage is 1 V across a series. The inset on the right-hand side shows spatial locations of the MTJ elements. The vector at each element shows the total magnetic field (amplitude and director) from the rest of the elements, calculated using Eq. (6). The zigzag trace indicates the current flow along the connected MTJ elements in a series. The inset on the left-hand side shows the coupling-induced noise as a function of the MTJ spacing. The knee is $\sim$30 μm.

varies along the series, the coupling-induced voltage noise of an N series will change as N increases. In Fig. 9, we show the coupling-induced voltage noise as a function of N in a series. The voltage noise is a sum of the all the noises from each element in the N series. As can be seen in Fig. 9, the coupling-induced noise initially decreases with N, then increases with N, followed by another decrease. Such behavior is in qualitative agreement with the experimental observation in Fig. 8(f). Magnetic coupling seems to have the tendency to amplify the magnetic noise in an N series. Efforts to reduce such a coupling will, therefore, benefit noise reduction in closely packed sensor arrays.

Additionally, we have calculated the coupling-induced noise as a function of the MTJ spacing as shown in the inset (left-hand side) of Fig. 9. Assuming that MTJ elements are positioned on a grid with equal horizontal and vertical unit vectors, the additional noise is found to exponentially decay with increasing MTJ spacing. The knee is $\sim$30 μm, after which an increase in space may lead to less reduction of the additional noise.

IV. CONCLUSION

In this paper, we carried out low-frequency noise measurements for two types of MTJ sensors connected in a series. The MTJ bridge sensor that comprised four arms in the Wheatstone bridge configuration showed a linear field response. Ten bridge MTJs were measured individually for ensuring uniform sensing and noise properties. Connecting these MTJs in a series, the magnetic field noise is found to decrease as the number of bridges increases. However, the total noise does not follow the $\sqrt{1/N}$ rule, possibly due to the statistical dispersion in MTJ bridge resistance and normalized voltage noise. In the second type of sensor array, a series of MTJ discrete resistors exhibit a strong correlation between the low-frequency magnetic noise and field sensitivity. Again, the total noise does not follow the $\sqrt{1/N}$ rule, but shows a sinusoidal-like variation with an increasing N in the series. We conjecture that magnetic coupling between the MTJ elements in the series is partially responsible for the N dependence of the total noise. Magnetic couplings between the MTJ elements tend to amplify the magnetic fluctuations, and should be minimized in any sensor design.

ACKNOWLEDGMENTS

At Brown University, the work was supported by National Science Foundation (NSF) under Grant No. DMR-0907353 and by Johns Hopkins University MRSEC under Grant No. DMR-0520491.

*wenzhe_zhang@brown.edu
†gang_xiao@brown.edu

[1] J. S. Moodera, L. R. Kinder, T. M. Wong, and R. Meservey, Phys. Rev. Lett. **74**, 3273 (1995).
[2] T. Miyazaki and N. Tezuka, J. Magn. Magn. Mater. **139**, L231 (1995).
[3] H. Xi, J. Loven, R. Netzer, J. I. Guzman, S. Franzen, and S. Mao, J. Phys. D **39**, 2024 (2006).
[4] C. T. Rogers and R. A. Buhrman, Phys. Rev. Lett. **55**, 859 (1985).
[5] A. S. Edelstein, J. Burnette, G. A. Fischer, S. F. Cheng, W. F. Egelhoff Jr., P. W. T. Pong, R. D. Mac Michael, and E. R. Nowak, J. Vac. Sci. Technol. A **26**, 757 (2008).
[6] A. S. Edelstein, G. A. Fischer, M. Pedersen, E. R. Nowak, S. F. Cheng, and C. A. Nordman, J. Appl. Phys. **99**, 08B317 (2006).
[7] A. Guedes, S. B. Patil, S. Cardoso, V. Chu, J. P. Conde, and P. P. Freitas, J. Appl. Phys. **103**, 07E924 (2008).
[8] M. Tondra, J. M. Daughton, D. Wang, R. S. Beech, A. Fink, and J. A. Taylor, J. Appl. Phys. **83**, 6688 (1998).
[9] R. Guerrero, M. Pannetier-Lecoeur, C. Fermon, S. Cardoso, R. Ferreira, and P. P. Freitas, J. Appl. Phys. **105**, 113922 (2009).
[10] W. Zhang, G. Xiao, and M. J. Carter, Phys. Rev. B **83**, 144416 (2011).
[11] F. N. Hooge, T. G. M. Kleinpenning, and L. K. J. Vandamme, Rep. Prog. Phys. **44**, 479 (1981).
[12] J. M. Almeida, P. Wisniowski, and P. P. Freitas, IEEE Trans. Magn. **44**, 2569 (2008).
[13] F. G. Aliev, R. Guerrero, D. Herranz, R. Villar, F. Greullet, C. Tiusan, and M. Hehn, Appl. Phys. Lett. **91**, 232504 (2007).
[14] A. Gokce, E. R. Nowak, S. H. Yang, and S. S. P. Parkin, J. Appl. Phys. **99**, 08A906 (2006).
[15] H. T. Hardner, M. B. Weissman, M. B. Salamon, and S. S. P. Parkin, Phys. Rev. B **48**, 16156 (1993).
[16] S. Ingvarsson, G. Xiao, S. S. P. Parkin, W. J. Gallagher, G. Grinstein, and R. H. Koch, Phys. Rev. Lett. **85**, 3289 (2000).
[17] C. Ren, X. Y. Liu, B. D. Schrag, and G. Xiao, Phys. Rev. B **69**, 104405 (2004).
[18] A. Ozbay, A. Gokce, T. Flanagan, R. A. Stearrett, E. R. Nowak, and C. Nordman, Appl. Phys. Lett. **94**, 202506 (2009).
[19] N. Smith, A. M. Zeltser, D. L. Yang, and P. V. Koeppe, IEEE Trans. Magn. **33**, 3385 (1997).